ISSN 1995-0780, Nanotechnologies in Russia, 2017, Vol. 12, Nos. 3–4, pp. 156–164. © Pleiades Publishing, Ltd., 2017.
Original Russian Text © E.V. Bessudnova, N.V. Shikina, M.S. Mel'gunov, Z.R. Ismagilov, 2017, published in Rossiiskie Nanotekhnologii, 2017, Vol. 12, Nos. 3–4.

Synthesis and Characterization of 3D Hierarchical Rutile Nanostructures: Effects of Synthesis Temperature and Reagent Concentrations on the Texture and Morphology

E. V. Bessudnova[a]*, N. V. Shikina[a], M. S. Mel'gunov, and Z. R. Ismagilov[a,b]

[a] *Boreskov Institute of Catalysis, Novosibirsk, 630090 Russia*

[b] *Institute of Coal Chemistry and Material Science Federal Research Center of Coal and Coal Chemistry, Kemerovo, 650000 Russia*

**e-mail: bev@catalysis.ru*

Received August 10, 2016; in final form, December 13, 2016

Abstract—Rutile nanostructures with a 3D hierarchical structure organization are synthesized via the sol-gel technique using $TiCl_4$ as a titanium precursor and HCl to regulate the acidity. The effects the synthesis conditions—molar ratios of the reagents ($[Cl^-]/[Ti^{4+}]$ and $[H_2O]/[Ti^{4+}]$) and temperature—have on the mechanism of formation of the rutile phase are established. We show that the texture and morphology of the rutile nanostructrures depend on the particle packing at all levels of the hierarchical organization and are directly related to the synthesis conditions.

DOI: 10.1134/S1995078017020045

INTRODUCTION

Titanium dioxide is a well-studied material that has found application in different nanotechnology-based industries, including nanobiotechnology. For applications in photocatalysis, lithium-ion cells, Gratzel's cells, and bionanomedicine [1–7], to name a few, TiO_2-based nanostructures must be thoroughly characterized; this includes information on their crystal structure, size, shape, and morphology (of the constituent particles). Much attention is therefore paid to the design of nanoscale TiO_2 architectures at the synthesis stage [8]. The sol-gel technique is currently one of the most commonly used synthesis routes for preparing TiO_2 nanostructures. In essence, it is the hydrolysis of titanium alkoxides or halides in water or a hydrochloric acid solution at 150–180°C, followed by deposition into an inorganic framework [9, 10]. The sol-gel synthesis route enables one to obtain a product with desirable properties by giving flexibility in adjusting the chemical nature of a precursor to be used, concentrations of reagents, and temperature and pH of the reaction medium. Controlling these parameters, a final product of high purity and homogeneity and with desirable size and morphology can be prepared at low temperatures [11, 12].

Titanium dioxide occurs in nature in three different polymorphs: anatase, brookite, and rutile—thermodynamically the most stable polymorph. Owing to its high refractive index, rutile is broadly used as a pigment in paint formulations and make-up products [13]. It is known that the high surface energy of rutile, as compared to anatase, makes it difficult to prepare rutile nanostrustures [14–16]. Thus, TiO_2 particles of 14 nm or less are thermodynamically more stable in anatase form, whereas, according to different estimates, the anatase-to-rutile phase transition takes place when the particle size is within the 14–70 nm range. Anatase and amorphous TiO_2 particles convert into rutile form at temperatures in excess of 450°C and when their size exceeds a certain critical value. At the temperatures of the polymorph transition, the particles agglomerate, which leads to a reduction in the specific surface area (SSA < 7 $m^2\ g^{-1}$).

The formation of highly hierarchical 3D structures is known to have a stabilizing effect on rutile structures [1]. Conventional approaches to the synthesis of rutile structures such as sol-gel, electrospray, hydro- and solvothermal methods, etc., yield flowerlike agglomerates that are typically 200–400 nm in diameter. The agglomerates represent ensembles of nanorods that themselves are chains of nanoparticles of 5–7 nm in diameter, which most likely are organized in a certain preferred manner (direction) [11]. Rutile nanostructures can be obtained from $TiCl_4$ at temperatures between 0 and 50°C via a solution–reprecipitation technique [17–19]. The morphology of the rutile particles has been shown to be strongly influenced by the initial concentration hydrochloric acid [11]. Spheroidal, cuboidal, flowerlike, cauliflower-like, and grapelike forms were observed, depending on the HCl concentration. The physical and chemical properties of the synthesized materials were defined by their

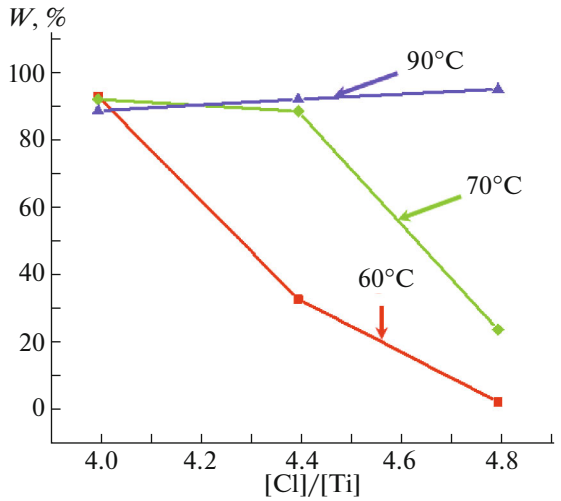

Fig. 1. (Color online) Rutile yield vs. the [Cl]/[Ti] ratio at different temperatures (60, 70, and 90°C) with $[H_2O]/[Ti^{4+}] = 39$.

(micro-)structure, i.e., overall shape, size, surface morphology, and anisotropy. Nowadays, synthetic strategies aimed at controlling the geometry of TiO_2 nanostructures in all three dimensions are the focus of research. Such materials possess a specific porous structure whose nature and pore volume and size distributions are well known. Texture is a key characteristic of TiO_2-based materials intended as catalyst supports. Properties of a hierarchical system with complex organization are mainly set by the properties of constituent particles and the peculiarities of their assembly.

In our early works, we demonstrated the possibility of synthesizing nanosized rutile structures at atmospheric pressure and temperatures below 100°C, with the temperature being a factor in the rutile phase formation [20, 21]. Here we provide a detailed study of the effects the synthesis parameters—temperature and molar ratios of the reagents ($[Cl^-]/[Ti^{4+}]$ and $[H_2O]/[Ti^{4+}]$)—exert on the morphology and texture characteristics of nanosized rutile materials.

EXPERIMENTAL

Rutile was prepared from $TiCl_4$ via the sol-gel method. A series of samples was prepared at a constant reagent ratio $[H_2O]/[Ti^{4+}] = 39$, three different temperatures (60, 70, and 90°C), and three different values of the $[Cl^-]/[Ti^{4+}]$ ratio (4, 4.4, and 4.8). Another series of sample was synthesized at a constant temperature of 70°C; a constant reagent ratio $[H_2O]/[Ti^{4+}] = 66.5$; and different $[Cl^-]/[Ti^{4+}]$ ratios (4, 4.2, 4.4, 4.6, and 4.8). The resulting white and turbid suspensions strutified into precipitate and a mother liquor at room temperature for a day. The precipitate was separated from the mother liquor and purified of chloride ions (predominantly) by using dialysis against distilled water, followed by drying in air at 100°C.

An X-ray diffraction (XRD) analysis of our samples was performed on a HZG-4C diffractometer in a continuous mode (Freiberger Prazisionmechanik) using a Co K_α monochromatic source ($\lambda = 1.79021$ Å) and scanning 2θ in the range of 20°–85°. The crystallite size was estimated applying the Scherrer equation for the (110) reflections at $2\theta = 31.0°$ (for rutile). Raman spectra of the TiO_2 were acquired on a RFS 100/S FT-spectrometer (Bruker) in the range of wavenumbers from 3600 to 100 cm^{-1}. Texture characteristics of dried samples such as SSA, pore volume, and pore size distribution were obtained by low-temperature nitrogen adsorption using an ASAP-2400 device (Micrometrics). Transmission electron microscopy in regular (TEM) and high-resolution (HRTEM) modes was performed on a JEM-2010 microscope (JEOL, Japan), with a unit-cell resolution of 0.14 nm and an accelerating voltage of 200 kV. Scanning electron microscopy (SEM) imaging was performed on a JSM 6460LV microscope operating at 25 kV.

RESULTS AND DISCUSSION

Hydrolysis of $TiCl_4$ at different temperatures is accompanied by phase transitions in the parental reaction medium. Mixing the reagents together produces a transparent solution that gradually turns into an opalescent sol and then into a white turbid (milky) suspension that eventually, when stirring is stopped, segregates into a clear liquid and a white precipitate at the bottom. Under strongly acidic conditions, at a high $[Cl^-]/[Ti^{4+}]$ ratio of 4.8, and a temperature of 60°C, the precipitate did not form until after 2.5–3 h of heating the reacting mixture; a similar situation took place at the synthesis temperature of 70°C. The formation of a copious precipitate occurred almost immediately after the solution was heated to 90°C, with the rutile yield being slightly higher in more acidic solutions. The rutile yield as a function of the $[Cl^-]/[Ti^{4+}]$ ratio at different synthesis temperature is plotted in Fig. 1.

With the increased solution acidity, at a synthesis temperature of 60°C and $[Cl^-]/[Ti^{4+}]$ ratio of 4, 4.4, and 4.8, the rutile yield comprised 93.8, 34.3, and 3.4%, respectively, while at 70°C the yield was 92.2, 88.7, and 25%, respectively. At 90°C, the rutile yield improves with the increasing $[Cl^-]/[Ti^{4+}]$ molar ratio.

The XRD analysis of the dried precipitate and the dry residue obtained by evaporating the supernatant showed that the former is the rutile form of TiO_2 and the latter contained predominantly the anatase form (data not shown). The diffractograms recorded in this study are similar to those previously reported by us [20]. The XRD analysis revealed that the rutile nanocrystals are 55–70 and 140–200 Å long in the (110) and (002) directions, respectively. Raman spectroscopy confirmed that, regardless of the synthesis tem-

perature and acidity, the precipitate formed is the rutile form of TiO_2, which was identified by the bands characteristic of the rutile lattice vibrations at 143 (B_{1g}), 447 (E_g), 612 (A_{1g}), and 826 (B_{2g}) cm^{-1}.

With the $[H_2O]/[Ti^{+4}]$ molar ratio of 66.5 and 39 and varying $[Cl^-]/[Ti^{+4}]$ from 4 to 4.8 at the constant temperature of 70°C, the effect of HCl on the rutile yield was not unambiguous (Fig. 2). Thus, increasing the $[Cl^-]/[Ti^{+4}]$ molar ratio (4, 4.4, and 4.8)—and an excess of water ($[H_2O]/[Ti^{+4}] = 66.5$)—improves the yield, reaching 100% at $[Cl^-]/[Ti^{+4}] = 4.8$. Conversely, at low $[H_2O]/[Ti^{+4}] = 39$, as the concentration of the HCl drops, the rutile yield increases, reaching a maximum of 92.2% at $[Cl^-]/[Ti^{+4}] = 4$.

Our experimental results suggest that the reaction mechanism, the formation of a certain TiO_2 polymorph, and its texture characteristics and morphology are affected by the reaction temperature and the molar ratios of the reagents.

As is known from previous studies, TiO_2 polymorphs such as rutile and anatase can be synthesized via hydrolysis; however, using hydrolysis, it is more difficult to prepare nanocrystals with rutile than anatase structure [22, 23].

$$TiCl_4 + 2H_2O \rightarrow TiO_{2(rut)} + 4HCl, \quad (1)$$

$$TiCl_4 + 2H_2O \rightarrow TiO_{2(anat)} + 4HCl. \quad (2)$$

The Gibbs free energy of reactions (1) and (2) is −59.32 and −54.29 kJ/mol, respectively, which means that they proceed spontaneously [23]. The difference between these quantities is only 4.03 kJ/mol. Although reaction (1) is energetically more favorable than (2), the latter is more kinetically facile at elevated temperatures [23]. Nonetheless, by varying several reaction conditions simultaneously—ratios of the reagents and temperature and duration of the hydrolysis—one can find combinations that make kinetics of either reaction (1) or (2) faster as a result of a reduction in their activation energy.

Many authors consider that the mechanism of formation of the rutile polymorph from aqueous $TiCl_4$ sols consists in the "aging" of the complex ion $[Ti(OH)_nCl_m]^{2-}$ ($n + m = 6$) [24–27], with n and m depending on the acidity and chloride concentration; m grows with the solution acidity, that is, with $[H^+]$ and $[Cl^-]$. According to the crystal field theory, Ti(IV) ($3d^0$ configuration) possesses octahedral coordination in both an aqueous solution and in a solid. In the aqueous $TiCl_4$ sol, $[Ti(OH)_2Cl_4]^{2-}$ represents an octahedron wherein Ti, a central atom, is coordinated to four in-plane chloride ions and to two hydroxide ion in the apexes. Upon dilution, the chloride ions are replaced with hydroxide ions to give $[Ti(OH)_4Cl_2]^{2-}$. A pH < 3.5 and the synthesis temperature of 95°C, the surface of rutile nuclei found both in the aqueous $TiCl_4$ solution and in the sol is protonated.

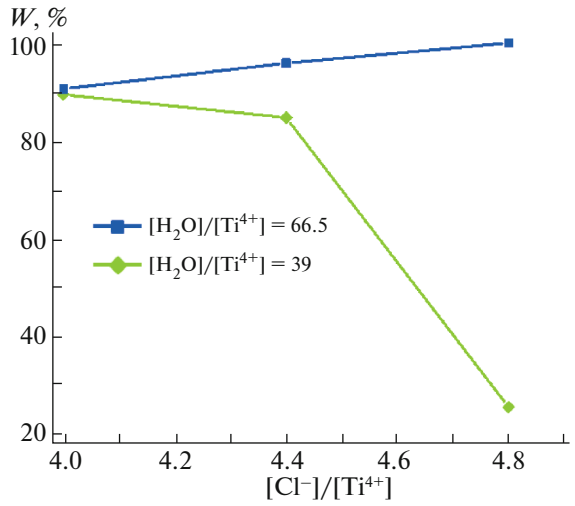

Fig. 2. (Color online) Rutile yield vs. the $[Cl^-]/[Ti^{4+}]$ ratio at different $[H_2O]/[Ti^{4+}]$ ratios (66.5 and 39) and the temperature of 70°C.

The formation of the nanocrystalline rutile polymorph can be depicted as follows: rutile nuclei combine with the complexes under discussion as a result of (i) water-molecule elimination from the OH^- ions through the oxolation reaction and (ii) the elimination of HCl, whereby H^+ is taken from the nuclei and Cl^- from $[Ti(OH)_4Cl_2]^{2-}$. At higher chloride concentrations, a rutile nucleus, a combination of two octahedral complexes linked together, can coordinate Cl^-, which encourages the connection between the edges rather than the faces. In this way, in the course of hydrolysis, the growth of the anatase form is suppressed and the formation of rutile nanocrystals is promoted, since the anatase form is made up of TiO_6 octahedra with shared planes, while the rutile form has its octahedra connected through the edges [20, 24, 28]. This mechanism is in good agreement with our experimental data when the hydrolysis is carried out at 90°C. At a lower temperature (70°C), the reaction mechanism is still valid but at a greater excess of water in the reaction medium ($[H_2O]/[Ti^{+4}] = 66.5$). With an insufficient amount of water and increasing [Cl]/[Ti] ratio, we observed the formation of a mixture of the polymorphs and their nuclei, which is due possibly to competing reactions that lead to the formation of brookite, amorphous phase, and their predecessors.

Texture parameters of dried rutile samples depend on the synthesis conditions. Figure 3 shows the differential pore size distribution curves calculated via the Barrett–Joyner–Halenda (BJH) method. As can be seen, the porous structure of the materials is quite complex and mostly consists of 3–8 nm mesopores. In the first series of the samples, which were prepared with $[H_2O]/[Ti^{+4}] = 39$ and at 60°C, the fraction of

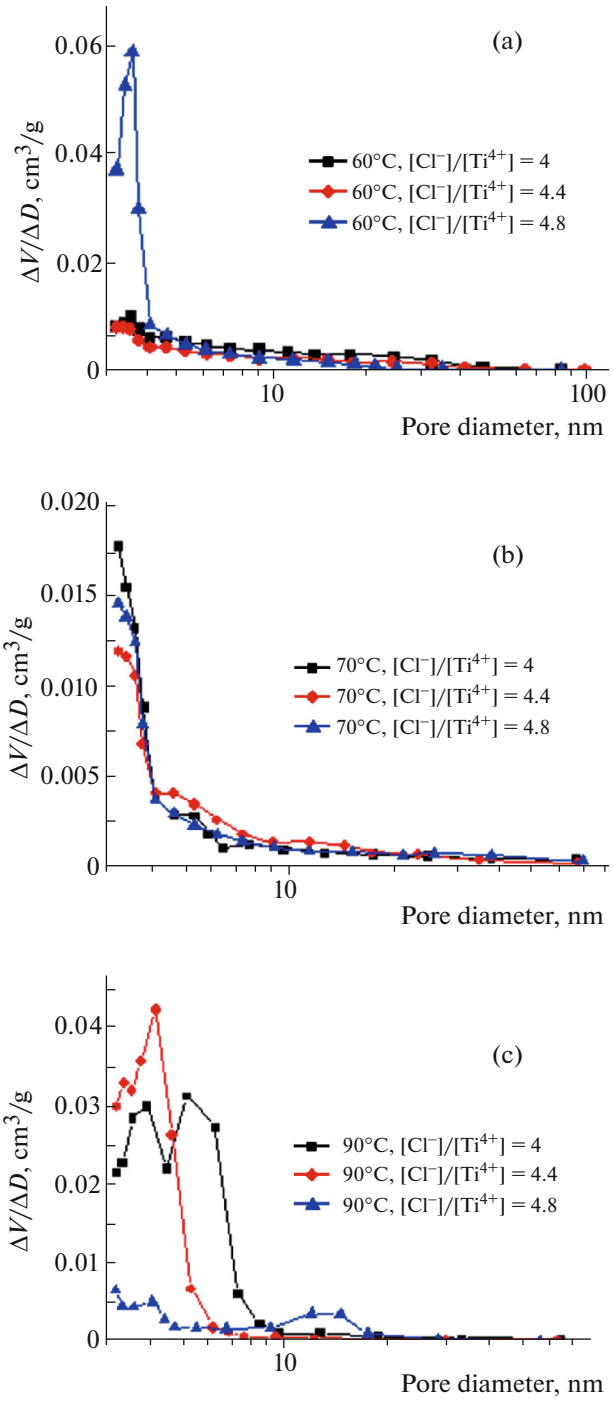

Fig. 3. (Color online) Differential pore-volume distributions of the rutile samples prepared at different [Cl$^-$]/[Ti^{4+}] ratios (indicated in the figure) and synthesis temperatures of (a) 60, (b) 70, and (c) 90°C.

mesopores with a size of 3.5–4 nm increases with the [Cl$^-$]/[Ti^{+4}] ratio up its maximum (Fig. 3a), whereas at 70°C the pore size is nearly independent of the [Cl$^-$]/[Ti^{+4}] ratio (Fig. 3b). At 90°C a distinct biporous structure occurs for all [Cl$^-$]/[Ti^{+4}] tried (Fig. 3c).

Key texture characteristics of the rutile samples prepared under different synthesis conditions (temperature, the [Cl$^-$]/[Ti^{+4}] and [H_2O]/[Ti^{+4}] ratios), which were derived from the low-temperature nitrogen adsorption data, are summarized in the table. Thus, according to the Brunauer–Emmett–Teller (BET) analysis, the SSA of the samples prepared at different hydrolysis temperatures grows with the [Cl$^-$]/[Ti^{+4}] ratio. At [H_2O]/[Ti^{+4}] = 39, the samples synthesized at 60 or 70°C have the highest SSA when [Cl]/[Ti] is 4.8, while for the 90°C samples the SSA is highest at the [Cl$^-$]/[Ti^{+4}] of 4.4. However, these relations are not always consistent with the pore-size distribution as derived from the BJH analysis. In characterizing a porous structure, one has to account for finer mesopores in the range of 2 to 3.5 nm—the range not included in the BJH method. As can be appreciated from the table, all the samples exhibit a trend to have their mesopore fraction increased when the [Cl$^-$]/[Ti^{+4}] ratio is raised from 4 to 4.8, which permits the conclusion that higher acidity leads to a denser material.

Unlike the samples prepared with the high [H_2O]/[Ti^{+4}] ratio of 66.5, those with [H_2O]/[Ti^{+4}] = 39.19 feature the presence of micropores that increase in number with the acidity, as can be seen from the adsorption isotherm shown Fig. 4. Increasing the medium acidity leads to (i) flattening adsorption isotherms (nearly parallel to the P/P_0 axis); (ii) a stronger displacement toward greater adsorption in the low-pressure region; and (iii) nearly vanishing hysteresis, which is characteristic of microporous materials. In fact, a denser material has more micropores in it.

By varying the synthesis parameters, one can obtain a material with SSA in the range of 110–190 m^2/g and with the pore volume of 0.1–0.2 cm^3/g.

Some of the key parameters characterizing nanostructured materials include the degree of crystallinity, domain size, number of defects, nature and stability of the surface. It has been recently reported that oxides having the rutile-type structure form nanorods that are made of spherical particles connected together along certain crystallographic directions [29]. Directional aggregation of particles begins with their self-organization, whereby they are aligned along some crystallographic orientation, followed by the attachment at the interface. Particle binding reduces the overall energy of the aggregates at the expense of the surface energy of uncompensated bonds of the primary particles, which thus leads to a more energetically favorable and coherent binding between the particles. This mechanism is equally valid for "free" particles and those having excess of adsorbed water at their surface. This process can allow for the difference

Texture characteristics of the rutile samples as affected by the synthesis conditions

T, °C	[Cl]/[Ti]	$[H_2O]/[Ti]$	a_{BET}, m^2/g	V_Σ, cm^3/g	Pore fraction with the size of 2–3.5 nm, %*	D, nm
60°C	4		159	0.20	27	3.8
	4.4	39.19	152	0.17	30	3.4
	4.8		190	0.18	42	3.7
70°C	4	39.19	138	0.13	46	3.8
		66.7	135	0.13	23	3.9
	4.4	39.19	119	0.12	42	3.9
		66.7	178	0.21	39	4.6
	4.8	39.19	152	0.14	49	3.6
		66.7	168	0.16	44	3.8
90°C	4		120	0.18	12	5.9
	4.4	39.19	149	0.13	30	3.6
	4.8		125	0.10	50	

*These pore sizes are not amenable to BJH analysis.

between various binding directions for the particles, whereas the (near-)surface oxygen vacancies may facilitate the specific adsorption of water molecules and the formation of surface hydroxyl groups. Synthetic rutile nanopowders with large SSA usually consist of associates of fine particles with numerous lattice defects. The preparation of nanocrystallites having a length of 80 ± 20 nm and diameter of 5–10 nm has been reported [11]; flowerlike agglomerates of these nanocrystalls with a size of 200–400 nm are morphologically similar to our samples.

A systematic analysis of the samples prepared at below 100°C with several electron microscopy techniques (TEM, HRTEM, and SEM) revealed that the nanostructured rutile samples have a complex packing arrangement and, owing to the characteristics described, fall into a category of 3D hierarchical structures [2]. At the first level of structural organization,

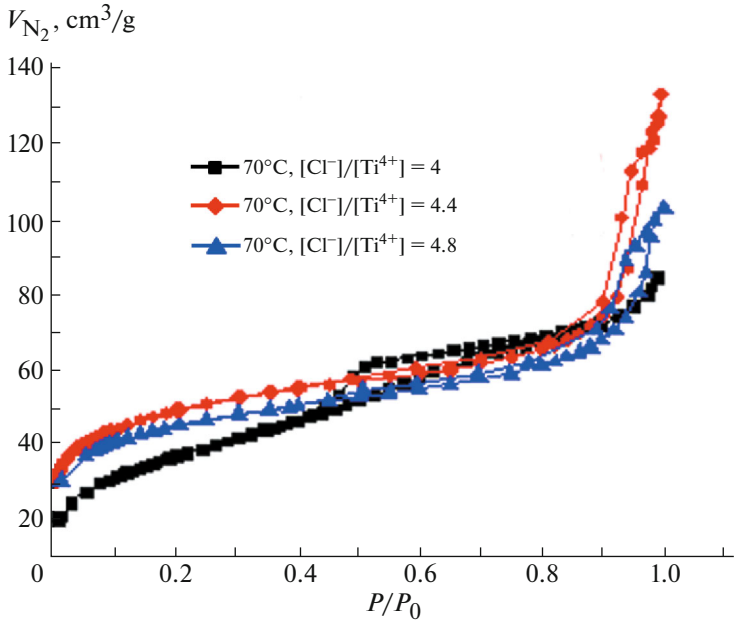

Fig. 4. (Color online) Adsorption and desorption isotherms for rutile samples prepared at different values of the $[Cl^-]/[Ti^{4+}]$ ratio, with $[H_2O]/[Ti^{4+}] = 66.5$ and a temperature of 70°C.

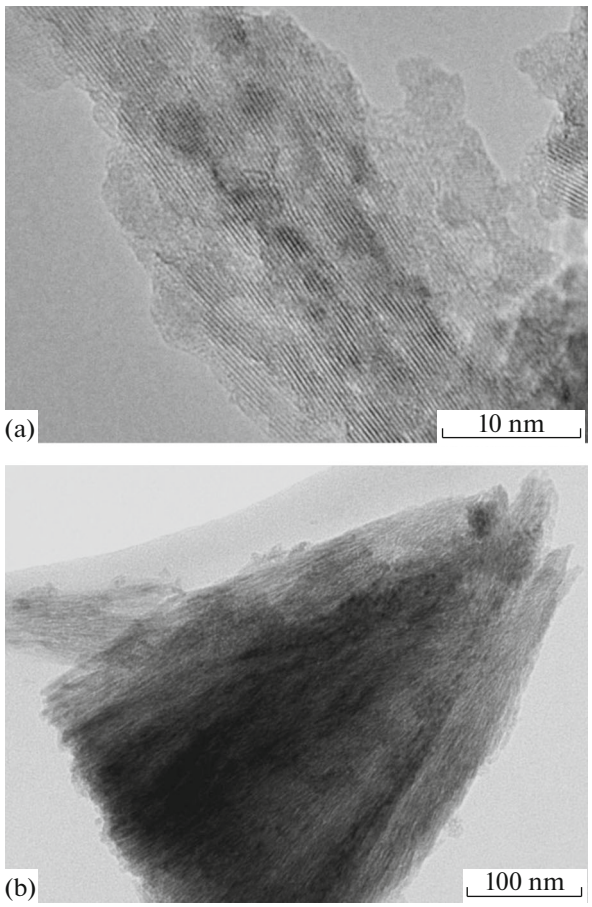

Fig. 5. (a) HRTEM image of coherently intergrown rutile nanoparticles and (b) TEM image of rutile nanofilaments bundled in fanlike aggregates.

the particles are coherently bound into filamentlike structures (Fig. 5a) which, in turn, are bundled in fanlike aggregates (Fig. 5b)—the second level of organization.

At relatively low synthesis temperatures (60 and 70°C) and a low $[Cl^-]/[Ti^{+4}]$ ratio, the aggregates appear as individual particles with a size from 10 to 100 nm. Raising the temperature to 90°C yields larger (up to 500 nm) and denser aggregates.

At the third level, the aggregates are organized into rather larger formations with a size of 1–8 μm (Fig. 6). The SEM images of the samples prepared at 60 and 70°C (Figs. 6a, 6b, 6d, 6e*)* show 6–8 μm particles of similar morphology reminiscent of a cauliflower. The synthesis conducted at 90°C yielded 1–1.5 μm structures of a spherical shape, which reduced the surface energy (Figs. 6c, 6f).

The effects the synthesis conditions have on the morphological features of the rutile were explored by varying the synthesis temperature, molar ratios of the reagents (Fig. 7).

Regardless of the acidity, raising the synthesis temperature from 60 to 90°C gives larger aggregates, as follows from TEM imaging (Figs. 7a → 7c and 7d → 7f). In acidic media and with higher $[Cl^-]/[Ti^{4+}]$ ratio of 4.8, there is a tendency to yield denser aggregates when compared to the case when $[Cl^-]/[Ti^{4+}] = 4$. These data corroborate the findings obtained with low-temperature nitrogen adsorption measurements. By comparing the TEM images of the different samples under discussion, we can conclude that raising the $[Cl^-]/[Ti^{4+}]$ ratio from 4 to 4.8 exerts a greater effect on the morphology at 60 and 70°C than at 90°C.

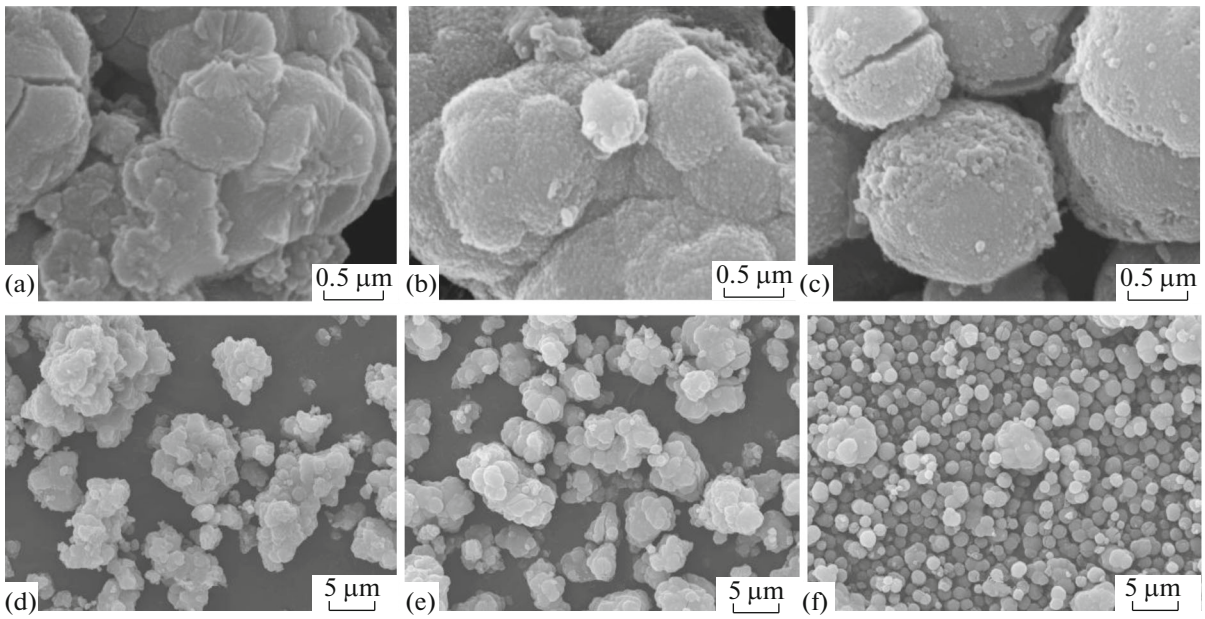

Fig. 6. SEM images of rutile samples synthesized at (a, d) 60, (b, e) 70, and (c, f) 90°C.

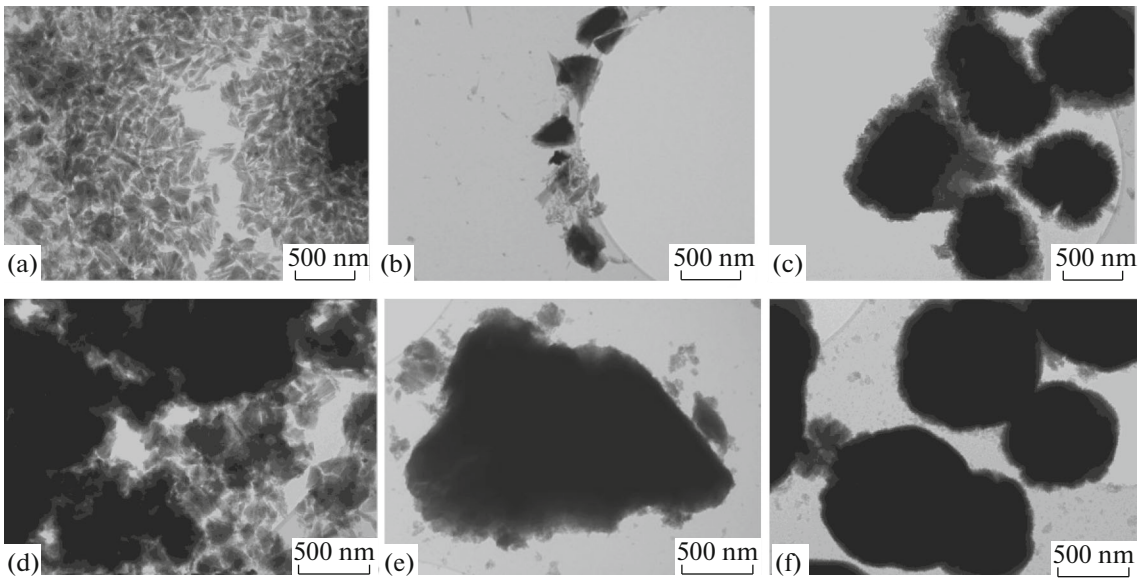

Fig. 7. TEM images of the rutile samples prepared at $[H_2O]/[Ti] = 39$, with [Cl]/[Ti] being (a–c) 4 and (d–f) 4.8. The synthesis temperature is (a, d) 60, (b, e) 70, and (c, f) 90°C.

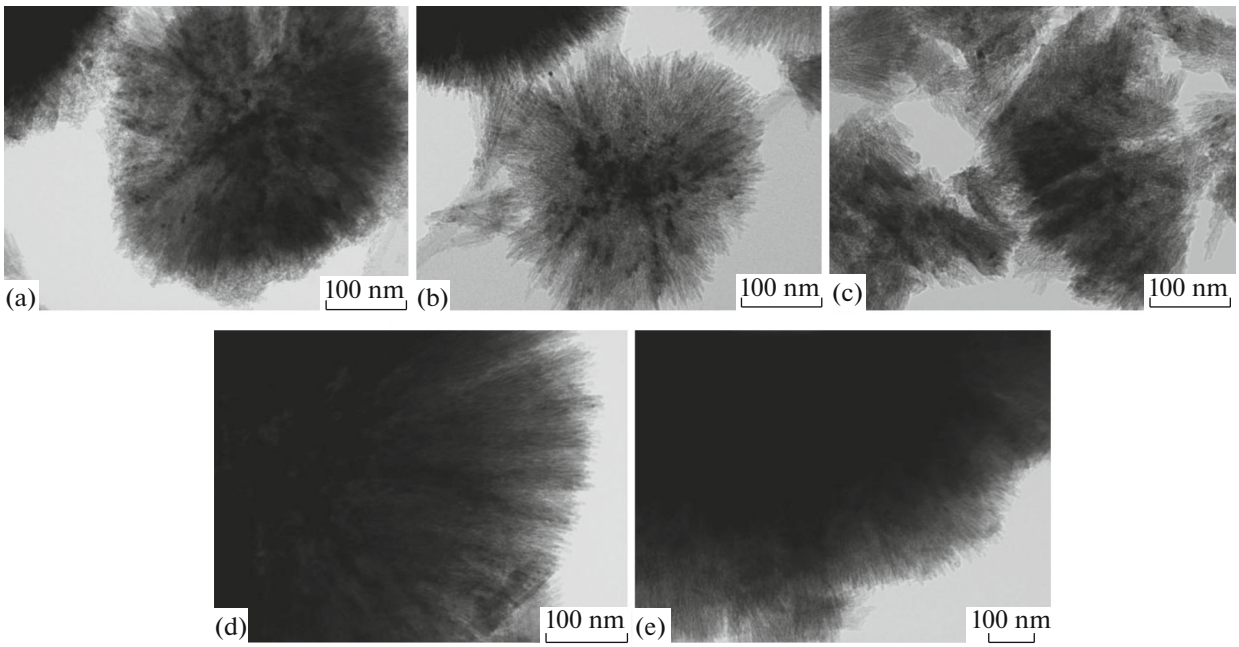

Fig. 8. TEM images of titanium dioxide samples synthesized at 70°C, the molar ratio $[H_2O]/[Ti^{4+}] = 66.5$, and variable [Cl]/[Ti] ratio: (a) 4, (b) 4.2, (c) 4.4, (d) 4.6, and (e) 4.8.

A series of the TEM images of the samples prepared at 70°C, $[H_2O]/[Ti^{+4}] = 66.5$, with a varying $[Cl^-]/[Ti^{4+}]$ ratio, is shown in Fig. 8. At the low values of $[Cl^-]/[Ti^{4+}]$ (4, 4.2, and 4.4), the aggregates formed are small and loose (Figs. 7a–7c). Raising the $[Cl^-]/[Ti^{4+}]$ ratio to 4.6 and 4.8 results in the formation of significantly lager and dense aggregates (Figs. 8d, 8e). These data also show a correlation with the nitrogen adsorption measurements (table).

Summarizing the experimental results, we can conclude that the specificities of the texture and morphology of the nanosized rutile samples synthesized herein are (i) determined by particle packing at all the levels of the structural hierarchy and (ii) strongly

depend on the synthesis conditions. Functional properties of the material are directly related to its crystal structure, texture, and the size and shape of the constituent particles [30–31]. Therefore, the exploration of the possibilities of controlling these parameters through adjustments of the synthesis conditions is of fundamental and practical significance.

CONCLUSIONS

We have developed a technique for synthesizing rutile with a highly porous and 3D hierarchical structure. The mechanism of the rutile phase formation is shown to be affected by all the synthesis parameters, i.e., the molar ratios of the reagents ($[Cl^-]/[Ti^{4+}]$ and $[H_2O]/[Ti^{+4}]$) and temperature. Varying one of the synthesis parameters affects the way the rutile yield as well as the texture and morphology depend on the other parameters. Studying the effects the synthesis parameters have on the structure and texture characteristics of the nanosized rutile, we found that increasing the temperature and acidity gives rise to rutile aggregates of greater size and increases the compactness (density) of the material. The mixed-type porous structure stems from the specific particle morphology. The particles are arranged in a complex multilevel structure: the filamentlike coherently intergrown crystallites stem radially from a common center and form fanlike aggregates that are packed into 3D structures having a form of intergrown or individual globules, which depends on the synthesis conditions. Regardless of peculiarities of the porous structure and morphology, the rutile samples, which were synthesized in a broad range of temperatures and molar ratios of the reagents, possess a developed surface (large SSA) and considerable porosity, which makes them prospective materials as catalyst supports.

ACKNOWLEDGMENTS

We are grateful to A.V. Ishchenko and N.A. Rudina for their help with physicochemical measurements.

This work was conducted within the framework of budget project no. 0303-2016-0004 for Boreskov Institute of Catalysis.

REFERENCES

1. D. Fattakhova-Rohlfing, A. Zaleska, and T. Bein, "Three-dimensional titanium dioxide nanomaterials," Chem. Rev. **114**, 9487–9558 (2014).
2. M. Marinaro, M. Pfanzelt, P. Kubiak, et al., "Low temperature behavior of TiO_2 rutile as negative electrode material for lithium-ion batteries," J. Power Sources **196**, 9825–9829 (2011).
3. K. Seki, "Catalyst for industrial HCl oxidation process," Catal. Surv. Asia **14**, 168–175 (2010).
4. A. N. Ozerin, A. N. Zelenetskii, T. A. Akopova, O. B. Pavlova-Verevkina, L. A. Ozerina, N. M. Surin, and A. S. Kechek'yan, "Nanocomposites based on modified chitosan and titanium oxide," Polymer Sci., Ser. A **48**, 638–643 (2006).
5. V. F. Zarytova, V. V. Zinov'ev, Z. R. Ismagilov, A. S. Levina, M. N. Repkova, N. V. Shikina, A. A. Evdokimov, E. F. Belanov, S. M. Balakhnin, O. A. Serova, S. I. Baiborodin, E. G. Malygin, and S. N. Zagrebel'nyi, "An examination of the ability of titanium dioxide nanoparticles and its conjugates with oligonucleotides to penetrate into eucariotis cells," Nanotechnol. Russ. **4**, 732 (2009).
6. N. A. Mazurkova, Yu. E. Spitsyna, N. V. Shikina, Z. R. Ismagilov, S. N. Zagrebel'nyi, and E. I. Ryabchikova, "Interaction of titanium dioxide nanoparticles with influenza virus," Nanotechnol. Russ. **5**, 417 (2010).
7. A. S. Levina, Z. R. Ismagilov, M. N. Repkova, N. V. Shatskaya, N. V. Shikina, F. V. Tuzikov, and V. F. Zarytova, "Nanocomposites consisting of titanium dioxide nanoparticles and oligonucleotides," J. Nanosci. Nanotechnol. **12**, 1812–1820 (2012).
8. H. Fei, M. Wei, R. Z. Shen, J. G. Wang, et al., "Facile synthesis of hierarchical nanostructured rutile titania for lithium-ion battery," Electrochim. Acta **56**, 6997–7004 (2011).
9. M. Ye, Zh. Chen, W. Wang, et al., "Large-scale synthesis and characterization of fan-shaped rutile TiO_2 nanostructures," Mater. Lett. **62**, 3404–3406 (2008).
10. T. D. N. Phan, H. D. Pham, T. V. Cuong, et al., "A simple hydrothermal preparation of TiO_2 nanomaterials using concentrated hydrochloric acid," J. Cryst. Growth **312**, 79–85 (2009).
11. M. I. Comor, N. D. Abazovic, I. A. Jankovic, D. J. Jovanovic, M. Stoiljkovic, D. V. Sojic, and B. F. Abramovic, in *Rutile: Properties, Synthesis, and Applications,* Ed. by J. Low (Nova Science, New York, 2012).
12. Z. R. Ismagilov, N. V. Shikina, N. A. Mazurkova, L. T. Tsikoza, F. V. Tuzikov, A. V. Ushakov, A. V. Ishchenko, N. A. Rudina, D. V. Korneev, and E. I. Ryabchikova, "Synthesis of nanoscale TiO_2 and study of the effect of their crystal structure on single cell responses," Sci. World J. **12** (2012). doi 10.1100/2012/498345
13. G. Pffaf and P. Reynders, "Angle-dependent optical effects deriving from submicron structures of films and pigments," Chem. Rev. **99**, 1963–1981 (1999).
14. H. Zhang and J. Banfield, "Thermodynamic analysis of phase stability of nanocrystalline titania," J. Mater. Chem. **8**, 2073–2076 (1998).
15. H. Zhang and J. Banfield, "Understanding polymorphic phase transformation behavior during growth nanocrystalline aggregates: insights from TiO_2," J. Phys. Chem. B **104**, 3481–3487 (2000).
16. A. A. Gribb and J. F. Banfield, "Particle size effects on transformation kinetics and phase stability in nanocrystalline TiO_2," Am. Mineral. **82**, 717–728 (1997).
17. A. S. Topalov, D. V. Sojic, D. A. Molnar-Gabor, B. F. Abramovic, and M. I. Comor, "Appl. photocatalytic activity of synthesized nanosized TiO_2 towards the degradation of herbicide mecoprop," Catal. B: Environ. **54**, 125–133 (2004).

18. B. F. Abramović, D. V. Sojic, V. B. Anderluh, N. D. Abrazović, and M. I. Comor, "Nitrogen-doped TiO_2 suspensions in photocatalytic degradation of herbicides mecoprop and (4-chloro-2-methylphenoxy)acetic acid using various light sources," Desalination **244**, 293–302 (2009).
19. N. D. Abrazović, L. Mirenghi, I. A. Jancovic, N. Bibic, D. V. Sojic, B. F. Abramović, and M. I. Comor, "Synthesis and characterization of rutile TiO_2 nanopowders doped with iron ions," Nanoscale Res. Lett. **4**, 518–525 (2009).
20. Z. R. Ismagilov, E. V. Bessudnova, N. V. Shikina, and V. A. Ushakov, "Effect of synthesis temperature on properties of nanoscale rutile with high surface area," Nanotechnol. Russ. **9**, 21 (2014).
21. E. V. Bessudnova, N. V. Shikina, and Z. R. Ismagilov, "Nanoscale titanium dioxide synthesized by sol-gel method," Al'tern. Energet. Ekol., No. 7, 39–47 (2014).
22. G. Li, Y. He, X. Zhang, and Sh. Hu, in *Rutile: Properties, Synthesis, and Applications,* Ed. by J. Low (Nova Science, New York, 2012), pp. 53–74.
23. Y. Z. Li, Y. N. Fan, and Y. Chen, "A novel method for preparation of nanocrystalline rutile TiO_2 powders by liquid hydrolysis of $TiCl_4$," J. Mater. Chem. **2**, 1387–1390 (2002).
24. H. B. Yin, Y. J. Wada, T. Kitamura, T. Sumida, Y. Hasegawa, and Sh. Yanagida, "Novel synthesis of phase-pure nano-particulate anatase and rutile TiO_2 using $TiCl_4$ aqueous solutions," J. Mater. Chem. **12**, 378–383 (2001).
25. H. Cheng, J. Ma, Z. G. Zhao, and L. Qi, "Hydrothermal preparation of uniform nanosize rutile and anatase particles," J. Chem. Mater. **7**, 663–671 (1995).
26. Q.-H. Zhang, L. Gao, and J.-K. Guo, "Preparation and spectral characterization of quantum-size titanium dioxide in the rutile phase," Chin. J. Inorg. Mater. **15**, 923–934 (2000).
27. D. Bahnemann, A. Henglein, and L. Spanhel, "Detection of the intermediates of colloidal TiO_2-catalysed photoreactions," Faraday Discuss. Chem. Soc. **78**, 151–163 (1984).
28. K. Yanagisawa and J. Ovenstone, "Crystallization of anatase from amorphous titania using the hydrothermal technique: effects of starting material and temperature," J. Phys. Chem. B **103**, 7781–7787 (1999).
29. R. L. Penn and J. F. Banfield, "Imperfect oriented attachment: a mechanism for dislocation generation in defect-free nanocrystals," Science **281**, 969–971 (1998).
30. M. Gratzel, "Mesoporous oxide junctions and nanostructured solar cells," Curr. Opin. Colloid Interface Sci. **4**, 314–321 (1999).
31. G. K. Mor, K. Shankar, M. Paulose, O. K. Varghese, and C. A. Grimes, "Enhanced photocleavage of water using titania nanotube arrays," Nano Lett. **5**, 191–195 (2005).

Translated by A. Cuharuc